International Journal of Nanoelectronics and Materials
IJNeaM
ISSN 1985-5761 | E-ISSN 2232-1535


# Synthesis and Characterization of Hematite $Fe_2O_3$ Nanofiller for Enhanced Dielectric and Microwave-Absorbing Properties in PTFE Composites

Bello Murtala Alhaji 1[ab], Raba'ah Syahidah Azis 2[ac*], Muhammad Kashfi Shabdin 3[a] , Nurul Huda Osman 4[a] and Abubakar Yakubu 5[d]

[a] *Department of Physics, Faculty of Science, University Putra Malaysia, 43400 UPM, Serdang, Selangor, Malaysia*
[b] *Department of Physics, Shehu Shagari College of Education, P.M.B. 2129 Sokoto, Sokoto State, Nigeria*
[c] *Institute of Nanoscience and Nanotechnology (ION2), Universiti Putra Malaysia, 43400 UPM Serdang, Selangor, Malaysia*
[d] *Department of Physics, Kebbi State University of Science and Technology, Aliero, Nigeria*
*∗ Corresponding author. Tel.: +603-97696666; fax: +603-97696666; e-mail: rabaah@upm.edu.my*

**ABSTRACT**

This paper presents the synthesis of hematite Fe2O3 nanofiller from mill scales and its application in polytetrafluoroethylene (PTFE) composites for enhanced dielectric and microwave-absorbing properties. The nanofiller was obtained through 9 hours of high-energy ball milling, resulting in a particle size reduction 43.6 to 11.05 nm. The PTFE/Fe2O3 composites were fabricated by dispersing different concentration of Fe2O3 nanofillers using the dry powder processing technique. The structural and morphological characterization of the nanofiller and PTFE/Fe2O3 composites was carried out using X-ray diffraction (XRD) and field emission scanning electron microscopy (FESEM), respectively. The composites' microwave absorption properties were analyzed utilizing vector network analyzer (VNA) measurements in the 8–12 GHz frequency range. Based on the findings from the results, as the percentage of filler increased from 5 to 15%wt, the composites' loss tangent and dielectric constant increased from 0.0272 to 0.0478 and 2.12 to 3.25, respectively, while their reduced signal transmission speed was between 2.21 and 2.07 x 108 m/s at 8 GHz and from 2.24 to 2.11 x 108 m/s at 12 GHz. These findings demonstrate that Fe2O3 nanoparticles are a suitable material for developing microwave-absorbing polymer composites within the 8–12 GHz frequency range.

**Keywords:** *Complex permittivity, Composites, Hematite nanofiller, Polytetrafluoroethylene*

## 1. INTRODUCTION

In recent years, there has been an increasing interest in the development of materials for electromagnetic interference (EMI) shielding. Among the various materials that have been investigated, composites made from polymers and magnetic particles have shown promising microwave-absorbing properties. These materials can effectively absorb electromagnetic waves and reduce EMI in electronic devices. Microwave absorbers (MA) are specifically designed to suit the needs of maintaining excellent absorption at a broad frequency range, having a thin thickness that can enhance microwave absorption properties [1], [2].

Physical and chemical assembly techniques can be employed to enhance designs by improving the performance of absorbent materials [3]–[7]. Microwave absorbers, which are used to attenuate electromagnetic (EM) waves, are typically fabricated using one-dimensional (1D) materials like carbon nanotubes [8], two-dimensional (2D) materials such as graphene [9], and more recently three-dimensional (3D) bulk materials like ferrites [10]. The different structural types result in varying surface areas, which in turn affect the interfacial polarization, scattering, and reflection of EM waves between surfaces. Magnetic losses and dielectric losses are two basic design requirements for microwave absorbers. Furthermore, ferrite is an important type of magnetic material composed of metal oxides containing magnetic ions, is particularly important due to its ability to achieve spontaneous magnetization while maintaining good dielectric properties [11]. Ferrites and other three-dimensional nanoparticles of metal oxide are prone to oxygen vacancy formation at the interfacial layers, which has an enormous impact on their magnetic and dielectric properties [12], [13]. The compactness of the nanoparticles allows for air-gap contact with the constituent particles, which increased interfacial polarization and hence complex permittivity. Ferrites are frequently synthesized by co-substitution using multistage chemical methods such as hydrothermal [14], solid state [15], co-precipitation [16], [17], and sol-gel [18], [19]. Hematite ($Fe_2O_3$), a ferrite with distinctive electrical and magnetic properties, is less frequently used for microwave absorption applications. A recent low-cost technique successfully synthesized $Fe_2O_3$ from industrially milled steel chips [20]–[22]. Hematite ($Fe_2O_3$) is inexpensive, environmentally friendly, and its dielectric loss properties can be improved by nanosizing the particles for use in polymer nanocomposites designed for applications in microwave absorption applications [23], [24].

On the other hand, polytetrafluoroethylene (PTFE) exhibits exceptional properties such as heat resistance at high and low temperatures, excellent dielectric properties, and chemical inertness, when compared to other polymers,

such as polyvinyl butyral, low-density polyethylene, polyphenylene sulphides, polyether ether ketone, and polystyrene [25].

However, the high thermal expansion coefficient of PTFE limits its practical applications. To address this limitation and enhance thermal and dimensional stability, various filler/PTFE composites have been developed. The effective incorporation of fillers has shown significant improvements in thermal and dimensional stability. PTFE has been used in numerous studies, including the development of Mg2SiO4-filled PTFE composites for microwave applications [26] and silicon dioxide ($SiO_2$) composites [27]. PTFE also demonstrates compatibility with natural fibers, modified glass fiber [28], and carbon fiber/epoxy composites [29]. The outstanding chemical inertness, high heat resistance, and notable dielectric properties of PTFE make it a suitable polymer matrix for incorporating different fillers in microwave applications. Combining PTFE, a non-conductive polymer matrix, with hematite ($Fe_2O_3$) enables the fabrication of a low-cost and lightweight magneto-dielectric absorber with favorable microwave absorption properties [24]. However, there is a lack of reports on the fabrication of nanocomposite materials comprising $Fe_2O_3$ and a PTFE matrix for electromagnetic and microwave applications.

In this study, a novel absorber with promising attenuation qualities for reducing electromagnetic interference reduction was developed by incorporating the $Fe_2O_3$ nanofiller with improved relative complex permittivity into a non-conductive PTFE polymer matrix. The nano-sized $Fe_2O_3$ NPs were obtained through high-energy ball milling (HEBM) using milled steel chips. The dry powder technique and hydraulic press, were used to mix $Fe_2O_3$ nanofiller ranging from 5 to 15 %wt. was mixed with the PTFE matrix to produce the nanocomposites. The effects of $Fe_2O_3$ loadings on the composition of PTFE/$Fe_2O_3$ and the complex permittivity and microwave reflection loss of the samples were also investigated. Furthermore, calculations and analyses were conducted on the signal propagation speeds in composites with various nanofiller contents.

## 2. MATERIALS AND METHODS

### 2.1. Materials

The mill scale chips were acquired from a steel factory in Malaysia. The polytetrafluoroethylene was purchased from Sanming (China-based Fujan Sannong New Materials Co., LTD) and utilized without further purification. The size of PTFE particles ranges from 50 to 110 μm.

### 2.2. Synthesis of Hematite ($Fe_2O_3$) NPs from industrial milled scale

Hematite ($Fe_2O_3$) was synthesized using industrially milled scale chips. The milled steel chips were initially prepared by extracting foreign and unwanted materials such as sand, dirt, stones, or pieces of plastic in order to prevent sample contamination. After that, the milled steel chips were washed, followed by drying in the oven and crushing using a pestle and mortar. Sizing processes were then carried out. About 200 g of mill scale waste is then weighed using an analytical balance (AY, 220) with an instrumental error of ± 0.00007 g for conventional ball milling. The flakes of mill scale were crushed into a fine powder to produce a magnetic wustite (FeO) slurry. Next, the slurry was processed by employing the magnetic separation method explained in [31, 32]. The slurry was then filtered and dried in an oven at 65°C for 24 hours. Furthermore, a carbolite furnace was used to oxidize the dry FeO at 600 °C for six hours to obtain $Fe_2O_3$ powder. The high-energy ball milling technique was utilized to mill $Fe_2O_3$ powder into nanoparticles in a SPEX8000D mill (Metuchen, SpexCertPrep, NJ, USA) at room temperature. The mill was powered at approximately 1425 revolutions per minute by a 50 Hz motor with a clamp speed of 875 cycles per minute and a ball-to-powder ratio of 1:5. The $Fe_2O_3$ nanoparticles were milled for 9 hours, as shown in Figure 1.

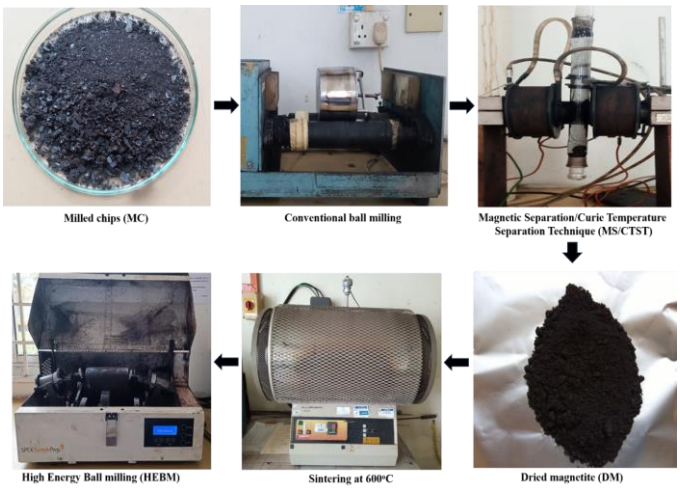


**Figure 1.** Synthesis procedure for Hematite ($Fe_2O_3$) nanoparticles from milled scale chips

### 2.3. Fabrication of PTFE/$Fe_2O_3$ Composite

The nanocomposites of PTFE/$Fe_2O_3$ were prepared by incorporating powdered PTFE with various $Fe_2O_3$ NPs with different mass ratios (5, 7.5, 10, 12.5, and 15%wt), according to Table 1. The composites of PTFE and $Fe_2O_3$ were made by mixing 5, 7.5, 10, 12.5, and 15%wt $Fe_2O_3$ filler with PTFE using a dry powder technique. The mixing process was undertaken for 10 minutes with a blender or wing mixer, and the content in each composite was set to 2.5 percent weight increments. The compositions were then pressed for 5 minutes, employing a hydraulic press with a 10 MPa pressure setting. The compressed composites were heated in a furnace at 3 ℃/min under room temperature to 380 ℃ and then maintained for 1 hour for the particles of the PTFE matrix to properly coalesce and fully eliminate voids. The sintering was performed using a furnace (Nabatherm GmbH Bahnhofstrasse, 2028865, Lilienthal, Germany). To complete the sintering cycle, the cooling rate from 380 ℃ to room temperature was set to 1.0 ℃ per minute. The rectangular waveguide's fitted sample has dimensions of 0.114 by 0.228 cm.

**Table 1.** Composition of $Fe_2O_3$/PTFE samples

| $Fe_2O_3$ Nanopowder | | PTFE | | Total mass (g) |
|---|---|---|---|---|
| Weight (%) | Mass (g) | Weight (%) | Mass (g) | |
| **5.0** | 1.50 | 95.00 | 28.50 | 30 |
| **7.5** | 2.25 | 92.50 | 27.75 | 30 |
| **10.0** | 3.00 | 90.00 | 27.00 | 30 |
| **12.5** | 3.75 | 87.50 | 26.50 | 30 |
| **15.0** | 4.50 | 85.00 | 25.25 | 30 |

### 2.4. Characterization of Synthesized Nano-Hematite and PTFE/$Fe_2O_3$ composites

#### 2.4.1 Structural, Morphological, and Elemental Composition Studies

Phase structure and composition of $Fe_2O_3$ nanoparticles, PTFE, and PTFE/$Fe_2O_3$ composites were analyzed at using an automated Philips X-pert system (Model PW3040/60 MPD, Amsterdam, The Netherlands) for X-ray diffraction (XRD) Cu-K radiation with a voltage of 40 kV, a current of 40 mA, and a wavelength of 1.5405 nm were utilized. The diffraction patterns in the 10 - 70° range were recorded at a scanning speed of 2 °/min. Rietveld analysis was performed on the data using Panalytical X'Pert Highscore Plus v3.0 software (PANalytical B.V., Almelo, the Netherlands). The $Fe_2O_3$ and PTFE/$Fe_2O_3$ composites' surfaces were examined using a FEI Nova Nano 230 field-emission scanning electron microscope (Kensington FESEM, Sydney, Australia) and X-ray energy-dispersive analysis (EDX). As the particle size decreases, the milling-induced strains result in a decrease in peak intensity and a widening of the diffraction peak's width. The average crystallite size (D), was estimated using Debye-Scherer's method given by equation (1) [30]:

$$D = \frac{0.94\lambda}{\beta \cos\theta} \quad (1)$$

where β represents the FWHM of the diffraction peak, λ is the wavelength of an X-ray, and θ is Bragg's angle of reflection.

#### 2.4.2 Signal Transmission Speed

The ability to transmit signals at a high speed with minimal delay is crucial for transmitting large amounts of data. Typically, when an electromagnetic wave propagates through a denser material, it is attenuated. Therefore, it is essential to study how filler content affects the speed of signal propagation in the process of designing microwave circuits with efficient data transmission. The signal transmission speed ($V_s$) can be estimated using the relation [31].

$$V_s = \frac{c}{\sqrt{\varepsilon' \mu'}} \quad (2)$$

Where c denotes the vacuum speed of light, $\varepsilon'$ represents the material's dielectric constant and $\mu'$ represents its permeability.

#### 2.4.3 Electromagnetic Properties

A rectangular waveguide (RWG) was employed to measure the complex permittivity and complex permeability within the frequency range of 8–12 GHz. The RWG was connected to a vector network analyzer (N5227A) (Agilent Technologies, USA, Santa Rosa) to conduct the measurements across the frequency range. During the experiment, it was critical to consider both the reflection and transmission of waves within the composites. The poly-reflection-transmission measurement technique was employed by the rectangular waveguide to measure the permittivity, $\varepsilon'$, and permeability, $\mu'$ of the samples. An optimization technique was utilized to ensure that the constant values of both $\mu'$ and $\varepsilon'$ were maintained throughout the entire frequency range. One significant advantage of the transmission-reflection technique is its ability to focus the field, enabling more accurate characterization of electromagnetic interference (EMI) characterization at microwave frequencies. For the vector analyzer, a typical full two-port calibration method was employed and 201 frequency points were set within the 8 to 12 GHz range. Additionally, using the VNA and a rectangular waveguide, the transmission-reflection of the samples with equal cross-sections at frequency range from 8 to 12 GHz frequency was determined, as depicted in Figure 2.

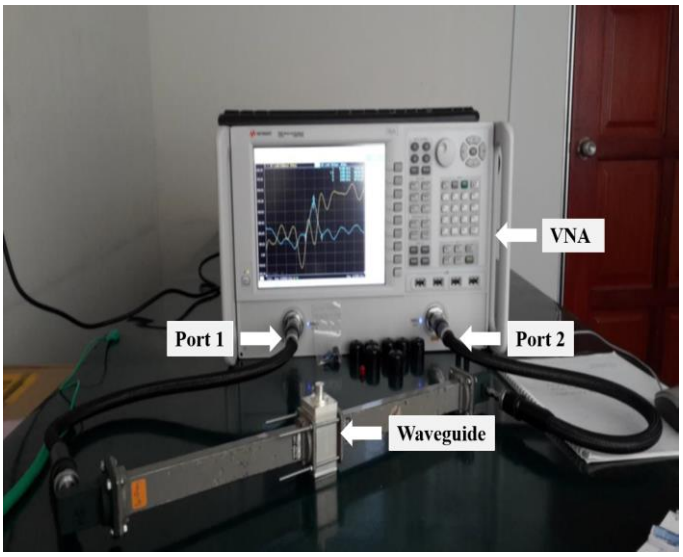


**Figure 2.** Measurement set up for Complex Permittivity.

## 3. RESULTS AND DISCUSSION

### 3.1. Characterization of Synthesized Hematite Nanoparticles and PTFE/$Fe_2O_3$ Composites X-ray Diffraction Pattern Analysis

Figure 3 displays the X-ray diffractograms of hematite ($Fe_2O_3$) particles after 9 hours of milling. Comparing the hematite ($Fe_2O_3$) diffraction patterns are compared to typical patterns in the ICSD (Inorganic Crystal Structure Database), it is evident that all Bragg peaks are consistent with the R—3 space group, indicating the rhombohedral

crystal structure of hematite, $Fe_2O_3$ (Reference code: 01-084-0309). Another phase is not detected, indicating that $Fe_2O_3$ did not transform into $Fe_3O_4$ during the ball milling process. The crystal structures of the 9-hour particles remained similar. Moreover, it was observed that the milled nanoparticles exhibited their highest intensity peaks in the (104) plane. This could be attributed to factors such as the ideal orientation [32], magnetic sequencing [33], or an increase in crystallinity due to ball milling. The PTFE XRD pattern in the same figure showed a sharp peak and five low-intensity peaks located at 2θ = 18.05°, 31.27°, 36.27°, 40.92°, 48.78°, and 55.93°, while a sharp peak is located at 18.05°. These peaks match the ICSD index of PTFE and correspond to the (100), (110), (200), (107), (108), and (210) planes, respectively, based on the ICSD index of PTFE (ICSD 00-047-2217) [31]. Additionally, the intensity of the peak located at 2θ = 18.05° slightly decreases with the addition of different percentages of $Fe_2O_3$ nanofiller are added to the PTFE matrix. The absence of unwanted peaks in the composites' pattern indicates that there was no chemical interaction occurred between the PTFE matrix and $Fe_2O_3$ nanofiller.

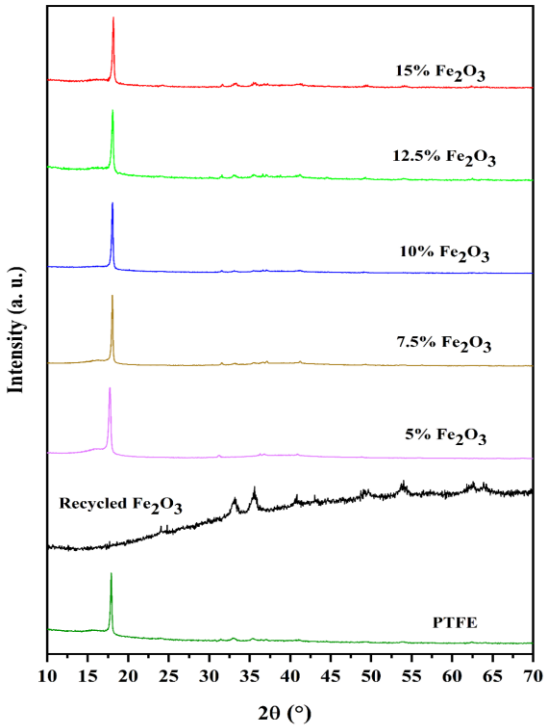


**Figure 3.** Diffractograms of X-rays of recycled $Fe_2O_3$, PTFE, PTFE/$Fe_2O_3$composites.

### 3.2. Analysis of Morphological and Elemental Composition Hematite NPs and PTFE/$Fe_2O_3$ composites

The FESEM image of the $Fe_2O_3$ nanoparticles after 9 hours of milling, PTFE, and $Fe_2O_3$/PTFE composites are depicted in Figures 4a-c, respectively. As the particles became underwent milling, they were refined into fine nanoparticles with noticeable aggregation and agglomeration [23]. The elemental compositions of $Fe_2O_3$ nanoparticles were determined using EDX, as shown in Figures 4a-c. The spectra of the nanoparticles revealed that they were composed of iron and oxygen. No impurities or other elements, were detected in the spectra indicating that the synthesized nanoparticles are pure iron oxides with no significant impurities. Figure 4a depicts the size distribution pattern of the 9-hour milled $Fe_2O_3$ particles. As the milling time increased, the peak center shifted towards the lower cross-sectional area of the particles [34]. The average grain size estimated from the 9-hours-milled $Fe_2O_3$ falls within the range of 16-12 nm. The spectra in Figure 4b show that PTFE is primarily composed of C (0.1 keV) and F (0.5 keV). In Figure 4c, it is evident that the $Fe_2O_3$ particles are uniformly distributed on the PTFE matrix exhibiting a pattern known as warts and dendrites that completely cover the surface of the PTFE matrix. These findings are consistent with previous research [35]. On the other hand, EDX was utilized to determine the elemental compositional of PTFE and PTFE/$Fe_2O_3$ composites. Further investigation reveals that the PTFE/$Fe_2O_3$ composites shown in Figure 4c contained both PTFE and $Fe_2O_3$ elements.

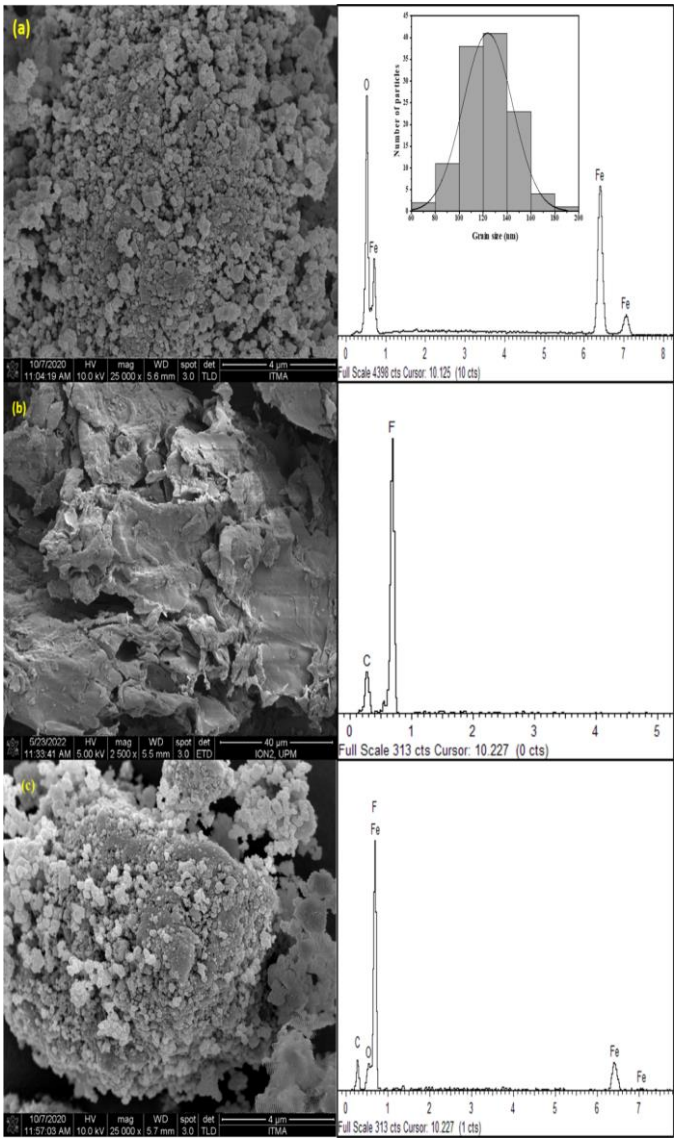


**Figure 4.** (a) FESEM images and EDX spectra for $Fe_2O_3$ after 9 h milling, (b) PTFE and, (c) PTFE/$Fe_2O_3$.

### 3.3. Complex Permittivity

Figure 5 depicts the dielectric constant ($\varepsilon'$) for PTFE/$Fe_2O_3$ composites within the measured frequency range. In Figure 5, the observed values of $\varepsilon'$ are 2.43, 2.45, 2.61, 2.63, and 3.25 for compositions of 5, 7.5, 10, 12.5 and 15 %wt., respectively, for the PTFE/$Fe_2O_3$ composites. The maximum value of $\varepsilon'$ for PTFE/$Fe_2O_3$ composites is found to be 3.25 for 15 %wt. On the other hand, the loss factors for the compositions of 5, 7.5, 10, 12.5, and 15 %wt. are 0.11, 0.14, 0.16, 0.18, and 0.24, respectively. It is concluded that the dielectric constant ($\varepsilon'$) and the loss factor ($\varepsilon''$) are enhanced with the increasing of the $Fe_2O_3$ nanofiller content in the matrix over the investigated frequency range. As predicted, the complex permittivity of composites increased when $Fe_2O_3$ nanofillers were loaded into the matrix, in accordance with the findings of previous studies on inorganic and organic matrix polymer composites [23], [36]. The complex permittivity characteristics of the material heavily depend on contributions from multiple polarizations, including electronic, interfacial, atomic, and orientation effects [37]. Additionally, the exchange of hopping between $O^{2-}$ and $Fe^{3+}$ within the localized states increases permittivity values [40, 41].

Further investigation revealed that $\varepsilon'$ and $\varepsilon''$ of PTFE/$Fe_2O_3$ composites increased as the $Fe_2O_3$ nanofiller size increased, which was consistent with previous work [40], [41]. This phenomenon attributed to increased density and interfacial polarization [42]. Composites reinforced with nanoparticles tend to have a larger interfacial area, resulting in an increase in interfacial polarization and dielectric properties [40], [43]. Furthermore, Figure 6 shows that the loss tangent increased significantly as the filler content increased from 5 to 15 wt.% within that frequency range, indicating that microwave attenuation properties of $Fe_2O_3$ improved with increasing filler content, which is consistent with previous work [44].

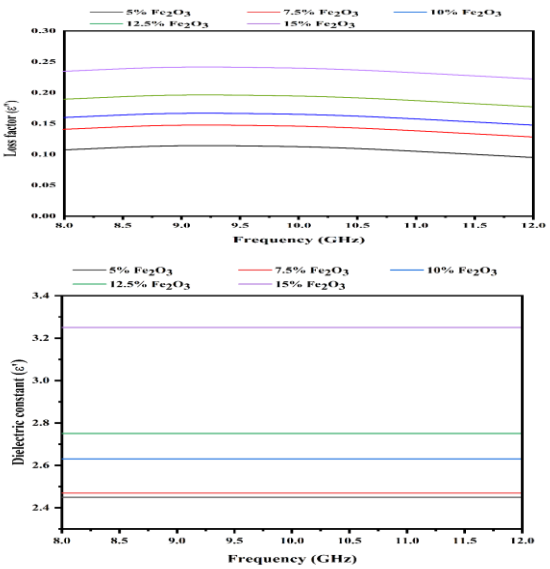


**Figure 5.** Complex permittivity of PTFE/$Fe_2O_3$ composites.

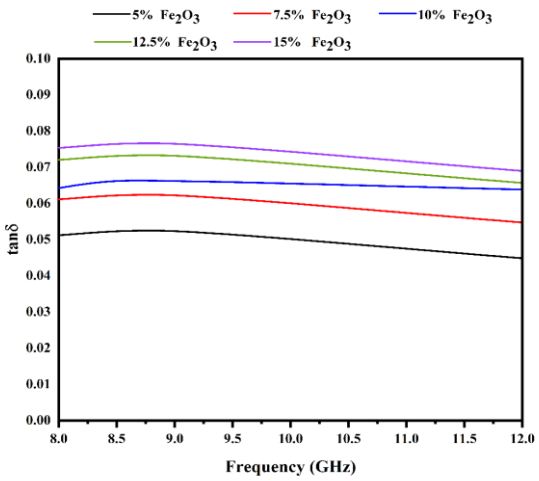


**Figure 6.** Loss tangent of PTFE/$Fe_2O_3$ composites

### 3.4. Speed of Signal Transmission

The variation in signal transmission speed through PTFE/$Fe_2O_3$ composites at various $Fe_2O_3$ mass percentages and frequencies is displayed in Figure 7. It is evident that the transmission speed reduces as the filler content increases. The relative permittivity of the filler content was found to be significantly lower at higher transmission speeds. The speed of signal transmission of PTFE/$Fe_2O_3$ samples at 8 and 12 GHz is presented in Table 2. As shown in Table 2, the velocity ($V_s$) of PTFE/$Fe_2O_3$ composites measured at 8 GHz decreases from 2.21 to 2.07 $\times 10^8$ m/s as the $Fe_2O_3$ filler content increases from 5 to 15%wt. At 12 GHz, the $V_s$ also decreases from 2.24 to 2.11 $\times 10^8$ m/s for the same filler ratio. At higher filler contents, the decreased transmission speed is substantially related to reduced relative permittivity [45].

**Table 2.** Speed of Signal Transmission of PTFE/$Fe_2O_3$ samples

| Weight (%) | $V_s$ ($\times 10^8$ m/s) | |
|---|---|---|
| | 8 GHz | 12 GHz |
| **5.0** | 2.21 | 2.24 |
| **7.5** | 2.20 | 2.22 |
| **10.0** | 2.18 | 2.21 |
| **12.5** | 2.15 | 2.17 |
| **15.0** | 2.07 | 2.11 |

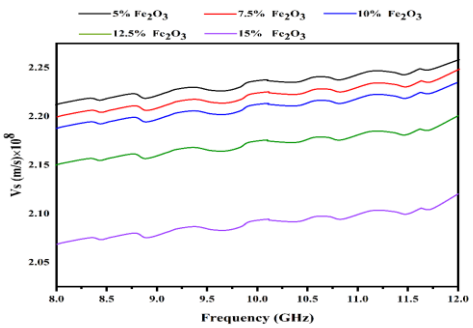


**Figure 7.** Signal transmission speed variation with increase in filler content

## 4. CONCLUSIONS

This research concludes by demonstrating the successful synthesis of hematite $Fe_2O_3$ nanofiller from mill scales and its application in PTFE composites for enhanced dielectric and microwave-absorbing properties. The use of 9 hours of high-energy ball milling resulted in the production of $Fe_2O_3$ nanoparticles with a size reduction of 11.05 nm. The prepared PTFE/$Fe_2O_3$ composites were characterized using XRD and FESEM techniques, while their microwave absorption properties were evaluated using VNA measurements in a frequency range of 8–12 GHz. The findings revealed that increasing the percentage of $Fe_2O_3$ nanofiller in the composite led to an increase in the loss tangent and dielectric constant while reducing the signal transmission speed. Overall, the study suggests that $Fe_2O_3$ nanoparticles are a promising material for developing microwave-absorbing polymer composites within the 8–12 GHz frequency range.

## ACKNOWLEDGMENTS

The authors would like to acknowledge the Department of Physics, Faculty of Science, Universiti Putra Malaysia for supplying the measurement facilities. The authors also acknowledge to the Fundamental Research Grant Scheme, Ministry of Higher Education Malaysia (MOHE), Grant No. FRGS/1/2023/STG07/UPM/02/8 for financing this research.

## REFERENCES

[1] D. K. Setua, B. Mordina, A. K. Srivastava, D. Roy, and N. Eswara Prasad, "Carbon nanofibers-reinforced polymer nanocomposites as efficient microwave absorber," in *Fiber-Reinforced Nanocomposites*, Elsevier, 2020, pp. 395–430.

[2] A. Yakubu, Z. Abbas, S. Abdullahi, S. Sahabi, and G. Sani, "Shielding Effectiveness, Mechanical and Dielectric Properties of NiO/PCL Nano Composites at Microwave Frequency for Electronic Devices," *J. Phys. Sci.*, vol. 25, no. 3, pp. 48–58, 2021.

[3] K. Zhang, X. Gao, Q. Zhang, H. Chen, X. C.-J. of M. And, and U. 2018, "Fe3O4 nanoparticles decorated MWCNTs@ C ferrite nanocomposites and their enhanced microwave absorption properties," *Elsevier*, vol. 452, pp. 55–63, 2018.

[4] I. R. Ibrahim et al., "A Study on Microwave Absorption Properties of Carbon Black and Ni0.6Zn0.4Fe2O4 Nanocomposites by Tuning the Matching-Absorbing Layer Structures," *Sci. Rep.*, vol. 10, no. 1, pp. 1–14, Feb. 2020.

[5] J. Mohammed et al., "Electromagnetic interference (EMI) shielding, microwave absorption, and optical sensing properties of BaM/CCTO composites in Ku-band," *Results Phys.*, vol. 13, p. 102307, Jun. 2019, doi: 10.1016/J.RINP.2019.102307.

[6] W. Chen, J. Wang, B. Zhang, Q. Wu, and X. Su, "Enhanced electromagnetic interference shielding properties of carbon fiber veil/Fe3O4 nanoparticles/epoxy multiscale composites," *Mater. Res. Express*, vol. 4, no. 12, Dec. 2017, doi: 10.1088/2053-1591/aa9af9.

[7] S. Kim, Y. Park, and S. K. C, "Double-layered microwave absorbers composed of ferrite and carbon fiber composite laminates," *Phys. stat. sol*, vol. 4, no. 12, pp. 4602–4605, 2007, doi: 10.1002/pssc.200777374.

[8] V. A. da Silva and M. C. Rezende, "Effect of the morphology and structure on the microwave absorbing properties of multiwalled carbon nanotube filled epoxy resin nanocomposites," *Mater. Res.*, vol. 21, no. 5, 2018, doi: 10.1590/1980-5373-MR-2017-0977.

[9] L. Huang et al., "Challenges and future perspectives on microwave absorption based on two-dimensional materials," *IEEE Trans. Microw. Theory Tech.*, vol. 72, no. 12, pp. 2719–2731, Dec. 2024, doi: 10.1109/TMTT.2024.2381231.

[10] A. Kanapitsas, C. Tsonos, G. C. Psarras, and S. Kripotou, "Barium ferrite/epoxy resin nanocomposite system: Fabrication, dielectric, magnetic and hydration studies," *Express Polym. Lett.*, vol. 10, no. 3, pp. 227–236, Mar. 2016. DOI: 10.3144/expresspolymlett.2016.21.

[11] M. R. Meshram, N. K. Agrawal, B. Sinha, and P. S. Misra, "Characterization of M-type barium hexagonal ferrite-based wide band microwave absorber," *J. Magn. Magn. Mater.*, vol. 271, no. 2–3, pp. 207–214, May 2004. DOI: 10.1016/j.jmmm.2003.09.045.

[12] F. Gözüak, Y. Köseoğlu, A. Baykal, and H. Kavas, "Synthesis and characterization of CoxZn1-xFe2O4 magnetic nanoparticles via a PEG-assisted route," *J. Magn. Magn. Mater.*, vol. 321, no. 14, pp. 2170–2177, Jul. 2009. DOI: 10.1016/j.jmmm.2009.01.008.

[13] E. R. Kumar and A. S. Kamzin, "Effect of particle size on structural, magnetic and dielectric properties of manganese substituted nickel ferrite nanoparticles," *J. Magn. Magn. Mater.*, vol. 378, pp. 389–396, Mar. 2015. DOI: 10.1016/j.jmmm.2014.11.019.

[14] M. H. H. Mahmoud and M. M. Hessien, "Microwave Assisted-Hydrothermal Synthesis of Nickel Ferrite Nanoparticles," *Orient. J. Chem.*, vol. 34, no. 5, pp. 2577–2582, Oct. 2018.

[15] S. A. Saleh, I. A. Abdel-Latif, A. M. A. Hakeem, and E. M. M. Ibrahim, "Structural and frequency-dependent dielectric properties of (SnO2)1−x(Fe2O3)x," *J. Nanoparticle Res.*, vol. 22, no. 2, pp. 1–12, Jan. 2020.

[16] V. A. Bharati, S. B. Somvanshi, A. V. Humbe, V. D. Murumkar, V. V. Sondur, and K. M. Jadhav, "Influence of trivalent Al–Cr co-substitution on the structural, morphological and Mössbauer properties of nickel ferrite nanoparticles," *J. Alloys Compd.*, vol. 821, p. 153501, Apr. 2020.

[17] L. B. de Mello, L. C. Varanda, F. A. Sigoli, and I. O. Mazali, "Co-precipitation synthesis of (Zn-Mn)-co-doped magnetite nanoparticles and their application in magnetic hyperthermia," *J. Alloys Compd.*, vol. 779, pp. 698–705, Mar. 2019.

[18] S. E. Shirsath, D. Wang, S. S. Jadhav, M. L. Mane, and S. Li, "Ferrites Obtained by Sol–Gel Method,"

in *Springer International Publishing*, Cham: Springer International Publishing, 2018, pp. 1–41.

[19] G. Xian et al., "Synthesis of Spinel Ferrite MFe2O4 (M = Co, Cu, Mn, and Zn) for Persulfate Activation to Remove Aqueous Organics: Effects of M-Site Metal and Synthetic Method," *Front. Chem.*, vol. 8, p. 177, Mar. 2020. DOI: 10.3389/FCHEM.2020.00177/BIBTEX.

[20] N. Daud et al., "Preparation and characterization of Sr1− xNdxFe12O19 derived from steel-waste product via mechanical alloying," *Mater. Sci. Forum*, vol. 846, no. 1662–9752, pp. 403–409, 2016.

[21] R. S. Azis, M. Hashim, N. M. Saiden, N. Daud, and N. M. M. Shahrani, "Study the Iron Environments of the Steel Waste Product and its Possible Potential Applications in Ferrites," *Adv. Mater. Res.*, vol. 1109, pp. 295–299, Jun. 2015.

[22] N. M. Shahrani, S. Raba'ah, M. Hashim, J. Hassan, Z. Azmi, and D. Noruzaman, "Effect of variation sintering temperature on magnetic permeability and grain sizes of Y3Fe5O12 via mechanical alloying technique," *Mater. Sci. Forum*, vol. 846, pp. 395–402, 2016.

[23] E. E. Mensah, Z. Abbas, R. S. Azis, N. A. Ibrahim, and A. M. Khamis, "Complex Permittivity and Microwave Absorption Properties of OPEFB Fiber–Polycaprolactone Composites Filled with Recycled Hematite (α-Fe2O3) Nanoparticles," vol. 11, no. 5, p. 918, May 2019.

[24] A. M. Khamis, Z. Abbas, R. S. Azis, E. E. Mensah, and I. A. Alhaji, "Effects of Recycled Fe2O3 Nanofiller on the Structural, Thermal, Mechanical, Dielectric, and Magnetic Properties of PTFE Matrix," *Polym. 2021, Vol. 13, Page 2332*, vol. 13, no. 14, p. 2332, Jul. 2021.

[25] P. Jiang and J. Bian, "Low dielectric loss BST/PTFE composites for microwave applications," *Int. J. Appl. Ceram. Technol.*, vol. 16, no. 1, pp. 152–159, Jan. 2019.

[26] T. S. Sasikala and M. T. Sebastian, "Mechanical, thermal and microwave dielectric properties of Mg2SiO4 filled Polyteterafluoroethylene composites," *Ceram. Int.*, vol. 42, no. 6, pp. 7551–7563, May 2016.

[27] Y. Yuan, J. Wang, M. Yao, B. Tang, E. Li, and S. Zhang, "Influence of SiO2 Addition on Properties of PTFE/TiO2 Microwave Composites," *J. Electron. Mater.*, vol. 47, no. 1, pp. 633–640, Jan. 2018.

[28] L. Zheng, J. Zhou, J. Shen, Y. Qi, and W. Chen, "Effects on the thermal expansion coefficient and dielectric properties of CLST/PTFE filled with modified glass fiber as microwave material," *Chinese Chem. Lett.*, vol. 30, no. 5, pp. 1111–1114, May 2019.

[29] E.-T. Park, Y. Lee, J. Kim, B.-S. Kang, and W. Song, "Experimental Study on Microwave-Based Curing Process with Thermal Expansion Pressure of PTFE for Manufacturing Carbon Fiber/Epoxy Composites," *Materials (Basel).*, vol. 12, no. 22, p. 3737, Nov. 2019.

[30] I. G. Shitu et al., "Influence of Irradiation Time on the Structural and Optical Characteristics of CuSe Nanoparticles Synthesized via Microwave-Assisted Technique," *ACS Omega*, vol. 6, no. 16, pp. 10698–10708, Apr. 2021.

[31] I. A. Alhaji, Z. Abbas, M. H. M. Zaid, and A. M. Khamis, "Effects of Particle Size on the Dielectric, Mechanical, and Thermal Properties of Recycled Borosilicate Glass-Filled PTFE Microwave Substrates," *Polym. 2021, Vol. 13, Page 2449*, vol. 13, no. 15, p. 2449, Jul. 2021.

[32] S. Guerrero-Suarez and Martin-Hernandez, "Magnetic anisotropy of hematite natural crystals: increasing low-field strength experiments," *Springer*, vol. 101, no. 3, pp. 625–636, Apr. 2012, DOI: 10.1007/s00531-011-0666-y.

[33] S. Neogi, U. Chowdhury, A. K. Chakraborty, and J. Ghosh, "Effect of mechanical milling on the structural and dielectric properties of BaTiO3 powders," *Micro Nano Lett.*, vol. 10, no. 2, pp. 109–114, Feb. 2015, DOI: 10.1049/mnl.2013.0751.

[34] M. Lutfor Rahman, S. Bhattacharjee, M. Sydul Islam, F. Zahan, B. Biswas, and N. Sharmin, "A study on the preparation and characterization of maghemite (γ-Fe2O3) particles from iron-containing waste materials," *vol. 8, no. 4, pp. 1083–1094*, 2020. DOI: 10.1080/21870764.2020.1812838.

[35] P. Glaris, J. F. Coulon, M. Dorget, and F. Poncin-Epaillard, "Thermal annealing as a new simple method for PTFE texturing," *Polymer (Guildf).*, vol. 54, no. 21, pp. 5858–5864, Oct. 2013. DOI: 10.1016/J.POLYMER.2013.08.011.

[36] M. Airimioaei et al., "Effect of particle size and volume fraction of BaTiO3 powders on the functional properties of BaTiO3/poly(ε-caprolactone) composites," *Mater. Chem. Phys.*, vol. 182, pp. 246–255, Oct. 2016. DOI: 10.1016/J.MATCHEMPHYS.2016.07.029.

[37] A. F. Ahmad, S. H. A. Aziz, Z. Abbas, D. M. Abdalhadi, A. M. Khamis, and U. S. Aliyu, "Computational and Experimental Approaches for Determining Scattering Parameters of OPEFB/PLA Composites to Calculate the Absorption and Attenuation Values at Microwave Frequencies," *Polym. 2020, Vol. 12, Page 1919*, vol. 12, no. 9, p. 1919, Aug. 2020.

[38] K. L. Pickering, M. G. A. Efendy, and T. M. Le, "A review of recent developments in natural fibre composites and their mechanical performance," *Compos. Part A Appl. Sci. Manuf.*, vol. 83, pp. 98–112, Apr. 2016.

[39] E. E. Mensah, Z. Abbas, R. S. Azis, N. A. Ibrahim, A. M. Khamis, and D. M. Abdalhadi, "Complex permittivity and power loss characteristics of α-Fe2O3/polycaprolactone (PCL) nanocomposites: effect of recycled α-Fe2O3 nanofiller," *Heliyon*, vol. 6, no. 12, p. e05595, Dec. 2020.

[40] S. Thomas, J. Kavil, and A. Mathew Malayil, "Dielectric properties of PTFE loaded with micro- and nano-Sm2Si2O7 ceramics," *J. Mater. Sci. Mater. Electron.*, vol. 27, no. 9, pp. 9780–9788, Sep. 2016. DOI: 10.1007/S10854-016-5043-Y.

[41] Y. C. Chen, H. C. Lin, and Y. Der Lee, "The Effects of Filler Content and Size on the Properties of PTFE/SiO2 Composites," *J. Polym. Res.*, vol. 10, no. 4, pp. 247–258, 2003. DOI: 10.1023/B:JPOL.0000004620.71900.16.

[42] C. Xie, F. Liang, M. Ma, X. Chen, W. Lu, and Y. Jia, "Microstructure and Dielectric Properties of PTFE-

Based Composites Filled by Micron/Submicron-Blended CCTO," *Cryst. 2017, Vol. 7, Page 126*, vol. 7, no. 5, p. 126, Apr. 2017. DOI: 10.3390/CRYST7050126.

[43] M. G. Todd and F. G. Shi, "Validation of a novel dielectric constant simulation model and the determination of its physical parameters," *Microelectronics J.*, vol. 33, no. 8, pp. 627–632, Aug. 2002. DOI: 10.1016/S0026-2692(02)00038-1.

[44] E. E. Mensah, Z. Abbas, R. S. Azis, and A. M. Khamis, "Enhancement of Complex Permittivity and Attenuation Properties of Recycled Hematite (α-Fe2O3) Using Nanoparticles Prepared via Ball Milling Technique," *Mater. 2019, Vol. 12, Page 1696*, vol. 12, no. 10, p. 1696, May 2019.

[45] R. Ratheesh and M. T. Sebastian, "Polymer–Ceramic Composites for Microwave Applications," *Microw. Mater. Appl. 2V Set*, pp. 481–535, Mar. 2017. DOI: 10.1002/9781119208549.CH11.